This is a repository copy of *Patient-Specific Biomechanical Modeling of Bone Strength Using Statistically-Derived Fabric Tensors*.

Article:

Patient-Specific Biomechanical Modeling of Bone Strength
using Statistically-Derived Fabric Tensors

Karim Lekadir[1,2], Christopher Noble[1,3], Javad Hazrati-Marangalou[5], Corné Hoogendoorn[1,2],

Bert van Rietbergen[5], Zeike A. Taylor[1,3], and Alejandro F. Frangi[1,4]

[1] Center for Computational Imaging & Simulation Technologies in Biomedicine

[2] Department of Information and Communication Technologies

Universitat Pompeu Fabra, Barcelona, Spain

e-mail: karim.lekadir@upf.edu

[3] Department of Mechanical Engineering

University of Sheffield, Sheffield, UK

[4] Department of Electronic and Electrical Engineering

University of Sheffield, Sheffield, UK

[5] Orthopaedic Biomechanics, Biomedical Engineering Department

Eindhoven University, Eindhoven, The Netherlands

Corresponding author:

Karim Lekadir

Universitat Pompeu Fabra

Department of Information & Communication Technologies

C/ Roc Boronat 138, 08018 Barcelona, Spain

Phone: +34 935 421 350, Fax: +34 935 422 927

E-mail: karim.lekadir@upf.edu

Abstract

Low trauma fractures are amongst the most frequently encountered problems in the clinical assessment and treatment of bones, with dramatic health consequences for individuals and high financial costs for health systems. Consequently, significant research efforts have been dedicated to the development of accurate computational models of bone biomechanics and strength. However, the estimation of the fabric tensors, which describe the microarchitecture of the bone, has proven to be challenging using in vivo imaging. On the other hand, existing research has shown that isotropic models do not produce accurate predictions of stress states within the bone, as the the material properties of the trabecular bone are anisotropic. In this paper, we present the first biomechanical study that uses statistically-derived fabric tensors for the estimation of bone strength in order to obtain patient-specific results. We integrate a statistical predictive model of trabecular bone microarchitecture previously constructed from a sample of ex vivo micro-CT datasets within a biomechanical simulation workflow. We assess the accuracy and flexibility of the statistical approach by estimating fracture load for two different databases and bone sites, i.e., for the femur and the T12 vertebra. The results obtained demonstrate good agreement between the statistically-driven and micro-CT-based estimates, with concordance coefficients of 98.6% and 95.5% for the femur and vertebra datasets, respectively.

Keywords: Bone fracture, finite element methods, bone microarchitecture, statistical predictive models, fracture load estimation.

1 Introduction

Fractures are amongst the most frequently encountered problems in the clinical assessment and treatment of bones [1,2]. Typically, fractures are caused by the application of a load that exceeds bone strength [3]. In particular, bones are susceptible to fracture even under small loads when the bone strength is affected due to bone abnormalities such as osteoporosis [4,5]. The pathology of osteoporosis is very common worldwide [6] and it is characterized by significant reduction in bone mass and deterioration of bone microarchitecture [7,8]. It is estimated that 1 out of 3 women and 1 out of 5 men are at risk of a low trauma fracture during their lifetime. Due to the dramatic health consequences for individuals [2,6] and the high financial costs for health systems [1], accurate prediction and effective prevention of low trauma bone fractures is of paramount importance.

To achieve this goal, techniques are required to assess the quality, and eventually the fragility, of bones. However, direct subject-specific estimation of bone strength using in vivo imaging remains challenging. Instead, significant research efforts have been dedicated to the development of computational biomechanical models of bones. With these models, one can simulate the behavior of the bone under different loading conditions and estimate the load that is required to cause the fracture of the bone, i.e. the fracture load, as an indicator of bone strength (for example, a large fracture load is an indication of high strength) [9,10,11,12,13,14,15]. These models are expected to play an important role in orthopedics for in silico personalized selection of bone-implant configurations that increase the strength/stability of the bones [16,17,18,19].

Because of the geometric and constitutive complexity of bones, stress/strain simulations are usually performed using advanced numerical tools such as the Finite Element (FE) method. However, the accuracy, and ultimately, the clinical translation of such computational biomechanical models depend currently on one essential requirement, i.e., that all the properties of the bone that contribute to its biomechanical function at both the macro- and micro-scale levels are estimated. Thus, it is important that the computational models include the trabecular microarchitecture, which is usually done by estimating the local fabric tensors [20,21,22]. Trabecular microarchi-

tecture has been shown to play an important role in determining bone quality and strength [23, 24, 25, 9, 26]. However, the subject-specific estimation of the fabric tensors requires in vivo imaging of the cancellous bone at high resolution, and this remains technically challenging. Micro-CT [27], for example, involves significant radiation and is thus limited to ex vivo research studies [28, 29]. On the other hand, high resolution peripheral quantitative CT (HR-pQCT) [30] is mostly used for the study of the distal parts of the skeleton (e.g., tibia and wrist) [30, 31, 32] and cannot be applied to more proximal or medial skeletal sites such as the femur and vertebra for which bone fractures are the most common.

As a consequence, most bone biomechanical studies have considered the tissue to be mechanically isotropic, as illustrated in these recent works [14, 33, 15, 16, 17, 34, 13], even though the material properties of bones are in essence orthotropic [35, 21, 36, 37]. Some methods have been proposed to estimate the trabecular fabric tensors directly from lower resolution imaging such as from clinical CT [38, 39, 40, 41]. However, such approaches can lack accuracy due to the microscopic scale of the trabeculae, and a recent study with the vertebrae produced inaccurate predictions both for the eigenvalues and eigenvectors of the fabric tensors [42]. Consequently, in vivo estimation of the trabeculae remains a challenge as highlighted in these recent review papers on fracture prediction [12] and implant design [18].

Recently, we presented the first statistical approach for the estimation of trabecular bone anisotropy based on a training database of ex vivo micro-CT datasets [43]. More specifically, predictive models were constructed to relate the known bone shape and density information to the missing trabecular fabric tensors. We addressed the large variability in vertebral microarchitecture by developing trabecula-specific predictive models with optimal predictor selection for each trabecular location. Furthermore, we developed a kernel-based nonlinear regression model to extrapolate the values of the unknown fabric tensors even in the presence of small training samples. This is particularly important due to the practical difficulties in finding large numbers of donors and thus in collecting large training ex vivo samples. Our results demonstrated

improved predictions of the fabric tensors over existing estimations [37] and consistent results across datasets.

In this paper, we extended our previous work with the following three objectives:

1) Firstly, we integrated the statistical predictive models of fabric tensors within a biomechanical simulation workflow that includes all important properties of the bones, i.e., shape, bone density, and micro-architecture. To the best of our knowledge, this is the first biomechanical study that uses statistically-derived fabric tensors for patient-specific simultion of bone biomechanics.

2) We evaluated whether the accuracy of the proposed statistical method for the estimation of fabric tensors translates into similar fidelity in the context of biomechanical simulations. For this, we also introduce a model for correcting the non-random bias due to the statistically-derived fabric tensors.

3) Finally, we assessed the flexibility and applicability of the proposed technique by running simulations for different databases and bone sites, i.e., the femur and the vertebrae. These bones have different geometric and functional properties. The femur is a long bone that is responsible for main body support, while the vertebrae are small bone structures that enter in the structural support and stability of the back. Both bone sites, however, are highly susceptible to bone fractures [1].

2   Material & Methods

In this study we performed FE simulations for a total of 53 bone samples, including 33 proximal femurs and 20 vertebral bones (T12). The goal was to compare the simulation results obtained from ex vivo high resolution micro-CT images with those estimated based on the statistically-derived fabric tensors. The inputs of our statistical predictive model are low resolution estimates of shape and bone density obtained from low resolution image data, while the outputs are the statistically-derived fabric tensors which are proposed as an alternative to micro-CT fabric tensors.

The outputs of the simulations are patient-specific FE models which account for bone heterogeneity and trabecular bone local anisotropy, which can be used to estimate fracture loads using existing failure criteria. Figure 1 summarizes schematically the main stages involved in this study, which are also detailed in the subsequent subsections.

Figure 1 appears here

Fig. 1 - Schematic diagram illustrating the main steps involved in the statistical approach for the estimation of fabric tensors, subsequently used in patient-specific biomechanical simulation and fracture load estimation. $\mathbf{X}$ represents the shape and bone density input variables of the statistical model, while $\mathbf{Y}$ represents the output (statistically-predicted) fabric tensors.

2.1 Datasets

Since high-resolution in vivo imaging of the bone trabeculae does not exist as yet, this study is performed based on cadaver bone datasets. More specifically, the simulations are run in this work for a total of 53 ex vivo micro-CT image data that include 33 proximal femurs and 20 T12 vertebrae (see Table 1 for a complete summary of the properties of the datasets). The donors had dedicated their body by testament to the Institute of Anatomy of the LMU in Munich or the Institute of Anatomy of the VU Amsterdam during life after Ethics approval for the purpose of teaching and research.

For the femur, 33 cases ex vivo micro-CT images were obtained from an online database [44] drawn from a population of 17 female donors and 16 male donors, and with an average age of 77.8 ± 10.0 years. The samples were initially stored in a buffered formalin solution. The images were acquired using micro-CT scans (XtremeCT, Scanco Medical AG, Brüttisellen, Switzerland)

of the most proximal part (~10 cm in length), with a nominal isotropic resolution of 82 µm. The images were filtered and processed according to the protocol recommended by the manufacturer.

The 20 donors for the vertebral bones consisted of ten male and ten female, with an average age of 78.0 ± 8.1 years (range 64-92 years). The T12 vertebrae were then scanned in a micro-CT system (microCT 80, Scanco Medical AG, Brüttisellen, Switzerland) at a nominal isotropic resolution of 37 µm using a 2048x2048 in plane image matrix. The scanner energy was 70 kV (114 µA).

2.2 Shape Extraction

The first stage of the simulation study involves the generation of subject-specific volumetric meshes of the bone morphology. We used a robust shape morphing approach that involved two stages, i.e., image segmentation and template mapping. Firstly, in order to define the trabecular bone, the original images were filtered and segmented using a thresholding procedure. For the femur, we applied a Laplace-Hamming filter (Laplace-epsilon = 0.5 voxel, Hamming-cutoff frequency = 0.4 voxel) and a segmentation threshold of 40% of the maximum possible value. For the vertebra, we used instead a strong Gaussian filter (sigma = 5, support = 5 voxels) and a threshold of 15% of the maximum gray-value. The difference in the filtering method is due to the higher-resolution of the vertebral images, for which a strong Gaussian filter is suitable. In contrast, the Laplace-Hamming filter is used for the femur because it better preserves the structures at such resolution.

Additional, the most periosteal 1 mm region of the trabecular bone as obtained from the thresholding was removed from the trabecular region, to ensure that no partial cortical bone is considered as trabecular bone.

Subsequently, we applied shape morphing to obtain the volumetric meshes for all bones with point correspondence (i.e., each element number identifies an element that, with good approximation, is at the same specific anatomical location in all samples). We used previously developed reference mesh templates for both the femur [45] and the vertebra [9] as estimated from large

CT databases of bones presenting average morphological characteristics. The reference templates were then mapped onto the individual bones by using the thin plate spline technique [46]. Key anatomical markers were first manually defined on the segmented images (8 landmarks for the femur, 20 for the vertebra). Finally, the obtained meshes consisted of 70,776 and 51,119 tetrahedral elements for the femur and the vertebra, respectively.

2.3 Bone Density

To derive the values of the bone density, a subsampling of the high resolution images was performed based on a new resolution of 4 mm. At each element centroid, a spherical region of 4 mm in diameter was defined and the bone density for that region was determined from the segmented micro-CT scans as the fraction of bone voxels over the total number of voxels in the spherical region.

2.4 Micro-CT Fabric Tensors

The fabric tensors were firstly quantified from the high-resolution micro-CT images to serve as the reference results for the evaluations and for statistical model training. For all the elements of the volumetric meshes, we calculated in the micro-CT images the Mean Intercept Length tensor [21] based on the same spherical regions from previous section, using the software accompanying the microCT scanner (IPL, Scanco Medical AG, Brüttisellen, Switzerland).

It is important to note that no fabric was calculated for cortical bone in this study. Instead, a unit fabric tensor was defined for cortical bone elements. Furthermore, the density of the cortical bone was determined as the fraction of bone voxels over the total number of voxels within the element volume.

2.5 Statistical Fabric Tensors

In this section we briefly describe the statistical approach used to estimate the fabric tensors. The fundamental idea was to determine statistically the relationship between the low resolution information found in clinical bone imaging such as CT (i.e., shape and density) and the trabecular

fabric tensors as extracted from high-resolution image data (micro-CT in our case). The estima-tion of high resolution information from lower resolution image data is a well-known problem in computer vision [47, 48]. In our work, we used a database of N ex vivo micro-CT datasets as a training sample to build the statistical predictive model, by following four main stages: 1) fabric tensor alignment, 2) fabric tensor transformation, 3) optimal selection of shape/density predic-tion, and 4) construction of a nonlinear regression model.

The tensor alignment step of the algorithm was necessary in our work due to the differences in shape and pose between the acquired datasets. To resolve this issue, all fabric tensors were re-oriented within a common coordinate system before the actual construction of the statistical model was carried out. More specifically, Procrustes analysis [49] was applied to align all the fab-ric tensors before subsequent statistical analysis by calculating the local rigid transformation be-tween corresponding tetrahedrons in the bone sample and in the reference mesh, and the obtained rotation matrices were then applied to reorient the eigenvectors of the fabric tensors.

Secondly, the proposed technique required a suitable mathematical representation of the fabric tensors, as they are symmetric tensors and thus lie on a Riemannian manifold [50]. This means we cannot use standard statistical tools, which can only be applied to variables that lie on Euclidean spaces, as this is not the case for symmetric tensors. To resolve this issue, we implemented the well-known Log-Euclidean framework in order to transform the tensor into an Euclidean space where the new variables can be manipulated using standard statistical tools. It has been shown that the following 6-D Log-Euclidean vector can be used [50]:

$$\mathbf{y} = (L_{11}, L_{22}, L_{33}, \sqrt{2}L_{12}, \sqrt{2}L_{13}, \sqrt{2}L_{23})^T. \tag{1}$$

where the L coefficients are the matrix logarithm components. More details can be found in Lekadir et al. [43].

Subsequently, for each individual local trabecular at each specific location of the bone, the shape and density predictors that correlate most with each fabric tensor were selected such that

the prediction power of the statistical model was optimized. For this, we constructed multiple

linear regressions to the data of the form:

$$\begin{aligned} \mathbf{y}_i^{(s)} &= \mathbf{a}_{ij} u_j^{(s)} + \mathbf{b}_{ij} + \mathbf{e}_{ij}^{(s)} \text{ (density)} \\ \mathbf{y}_i^{(s)} &= \mathbf{A}_{ij} \mathbf{v}_j^{(s)} + \mathbf{b}_{ij} + \mathbf{e}_{ij}^{(s)} \text{ (shape)} \end{aligned}. \tag{2}$$

where the upper index (s) denotes the sth sample in the training set. $\mathbf{a}_{ij}$, $\mathbf{A}_{ij}$, $\mathbf{b}_{ij}$ are the coeffi-

cients of the linear regressions, and $\mathbf{e}_{ij}^{(k)}$ is the residual vector of the regressions. We then meas-

ured the predictive power of each density and shape variable at element j for the prediction of

the fabric tensor at element i by calculating the squared sum of the prediction residuals:

$$r(\mathbf{y}_i \mid u_j \text{ or } \mathbf{v}_j) = \sum_{s=1}^{N} \mathbf{e}_{ij}^T \mathbf{e}_{ij}. \tag{3}$$

The bone shape and density variables with the lowest $r(\mathbf{y}_i \mid u_j \text{ or } \mathbf{v}_j)$ values were then selected

within the predictive model of each specific fabric tensor $\mathbf{y}_i$.

Finally, a non-linear regression model based on partial least squares regression (PLSR) [51], [52]

was estimated for the prediction of each local fabric tensor conditioned on the selected optimal

predictors. Given a new vector that encapsulates the shape and density predictors $\mathbf{x}_{new}$ and a ker-

nel Gramm function $\mathbf{K}$ used to unfold the underlying nonlinear relationships in the data, the un-

known fabric tensor $\hat{\mathbf{y}}_i$ at location i was predicted using the following equation:

$$\hat{\mathbf{y}}_i = \mathbf{K}(\mathbf{x}_{new})\mathbf{A}_i \tag{4}$$

where $\mathbf{A}_i$ is the optimal regression matrix calculated from the training data as:

$$\mathbf{A}_i = \mathbf{K}\mathbf{D}_i(\mathbf{C}_i^T \mathbf{K}\mathbf{D}_i)^{-1}\mathbf{C}_i^T \mathbf{Y}_i, \tag{5}$$

and $\mathbf{C}_i$ and $\mathbf{D}_i$ are the PLSR latent matrices. More details on the properties and implementation

of the kernel PLSR model can be found in [52].

The advantage of this regression technique is that it explicitly estimates the model parameters

that best fit the training data, which leads to statistically optimal predictions. Only weak a priori

assumptions are made about the type of relationship or model between the shape/density infor-

mation and the output tensors (i.e., that it is non-linear).

Following the statistical prediction of the missing fabric tensors, some incorrect or noisy predictions may be present within the resulting microarchitecture, for example due to noise in the input images. Therefore, as a final stage of our algorithm, we apply a mean filtering stage [53], which replaces each predicted fabric tensor value with the average tensor of its neighbors in the volumetric mesh, including itself. This has the effect of eliminating trabecular values which are unrepresentative of their surroundings due to noisy predictions. Let $V(i)$ be the set of neighboring elements for each trabecular element i in the volumetric mesh, as derived from the volumetric mesh (i.e., two elements are neighbors if they are connected by an edge in the tetrahedral mesh). The new smoothed tensor vector $\mathbf{y}_i^*$ is calculated from the previously calculated neighboring values $\hat{\mathbf{y}}_j$ ($j \in V(i)$) as follows:

$$\mathbf{y}_i^* = \frac{\displaystyle\sum_{j \in V(i)} w_{i,j} \hat{\mathbf{y}}_j}{\displaystyle\sum_{j \in V(i)} w_{i,j}} . \tag{6}$$

The weights $w_{i,j}$ are defined as the inverse of the distance between the elements at locations i and j in the volumetric mesh to take into account the relative proximity of the neighbors during the smoothing.

2.6 Finite Element Simulations

FE-based simulations of simplified femoral and vertebral physiological loading scenarios were performed to allow estimation of fracture loads for each subject. In each case, two simulations were performed, one using micro-CT- and the second using statistically-derived distributions of fabric tensors. Element-wise fabric tensors estimated using each method were converted into fourth order compliance tensors, for use in FE computations, using the formulation of Zysset and Curnier [22]. All simulations were performed using the ANSYS FEA package (www.ansys.com). Deformations were assumed to remain in a small strain range, and correspondingly linear elastic analyses were performed throughout. Both femur and vertebra FE meshes were generated using mesh templates from previous studies [9, 37, 44, 54], wherein mesh convergence analyses were also

undertaken. The computational meshes for vertebra models employed 10-node tetrahedron elements, and so a standard displacement-based element formulation with quadratic shape functions (known to give reliable results [55]) was used. Femur meshes were constructed of 4-node tetrahedron elements and a mixed displacement-pressure formulation was chosen to ensure reliable results [56].

For femur datasets, nodes on the distal (cut) surfaces of the models were fully constrained. Static loads of 1000 N [57], distributed over a small patch of nodes and with directions approximately normal to the bone surface, were applied to the femoral heads in the vicinity of the fovea capitus, emulating pelvic loading. For the vertebral datasets, an axial compression scenario was simulated, in which superior vertebral surfaces were fixed and inferior surfaces were displaced vertically by 0.5 mm [57].

2.7 Estimation of Fracture Load

Simulation results were firstly compared on the basis of principal strain ε_i and stress σ_i ($i = 1, 2, 3$) distributions within the models. Subsequently, these results were used to estimate the fracture loads for each subject following an approach similar to that of Pistoia et al. [57]. In this scheme, local failure of the bone tissue was assumed to occur when it exceeds the material-dependent critical value of a relevant failure criterion. We employed a maximum principal strain (MPS) criterion previously formulated and validated by Schileo in this work [58]. More specifically, bone tissue was assumed to exhibit tension/compression asymmetry such that failure occurs when either $|\varepsilon_1| > 0.0073$ or $|\varepsilon_3| > 0.0104$. This criterion has been shown to be an excellent predictor of bone tissue failure in ex vivo femur experiments [58]. Given the quasi-brittle nature of bone [59, 60], and of trabecular bone in particular, organ-level fracture (i.e. fracture of the bone as a whole, rather than localized failure of individual trabeculae) was then assumed to occur when > 5% of the elements in the mesh reach failure. We identified the external load level required to produce this state as the fracture load F. Since linear analyses were performed, simple scaling

of the model loads (or of reaction forces in the case of imposed displacements) and of corresponding solutions was required to estimate the fracture load in each case.

Using this approach, we obtained for each dataset $1 \leq k \leq N$ in the training sample a micro-CT fracture load $F_{\mu CT}^{(k)}$ and a statistically-based fracture load $F_{stat}^{(k)}$. For the leave-one-out tests performed in this study (i.e., the dataset used for verification was not included for the training of the models), $N = 32$ for the femur datasets and $N = 19$ for the vertebrae.

Due to the differences in the two types of fabric tensors, and more particularly to the smoothing effect that is common to statistical methods, a systematic (non-random) bias can be expected between the two fracture load values. More specifically, while the micro-CT models properly incorporate the discontinuities and transitions between the trabeculae found in the real tissue, the statistical model produces smooth bone micro-architectures. This is due to the PLSR prediction, which like any other eigen-decomposition dimensionality reduction technique, removes small (noisy in the statistical sense) components of variability during the predictions. The tensor filtering stage, which is effective for correcting potentially erroneous trabecular predictions, also contributes to more continuous bone microarchitectures than the ones quantified with micro-CT. When the resulting fabric tensors are used within simulations, these phenomena lead to a systematic over-estimation of the fracture load. Fortunately, unless for random prediction errors, systematic bias can be easily corrected for with different techniques that exist in the literature [61, 62]. Here, we used a simple linear regression to obtain the final estimated fracture load $F_{est}^{(k)}$ as follows:

$$F_{est} = \alpha F_{stat} + \beta, \tag{7}$$

where the systematic bias correction parameters α and β were computed such that the differences between $F_{est}^{(k)}$ and $F_{\mu CT}^{(k)}$ were minimized over the training sample, resulting in:

$$\alpha = \frac{N \sum_{k=1}^{N} F_{stat}^{(k)} F_{\mu CT}^{(k)} - \sum_{k=1}^{N} F_{stat}^{(k)} \sum_{k=1}^{N} F_{\mu CT}^{(k)}}{N \sum_{k=1}^{N} (F_{stat}^{(k)})^2 - (\sum_{k=1}^{N} F_{stat}^{(k)})^2}, \tag{8}$$

$$\beta = \frac{1}{N}(\sum_{k=1}^{N} F_{\mu CT}^{(k)} - \beta \sum_{k=1}^{N} F_{stat}^{(k)}). \qquad (9)$$

3   Experimental Results

In this section, we compared the simulation results obtained using i) the fabric tensors extracted from micro-CT and ii) those predicted using the proposed statistical approach. For the proposed statistical method, all experiments were performed using a leave-one-out approach. For each dataset, we obtained a fracture load $F_{\mu CT}^{(k)}$ based on the fabric tensors extracted from micro-CT and another fracture load $F_{est}^{(k)}$ by using the proposed statistical method (Eq. (7)). We then calculated the following relative error measure for each dataset:

$$\frac{|F_{est}^{(k)} - F_{\mu CT}^{(k)}|}{F_{\mu CT}^{(k)}}.100\% . \qquad (10)$$

Additionally, we quantified the agreement in the estimation of the fracture loads between the micro-CT and statistical models based on the concordance correlation coefficient (ρ_c) [63].

3.1 Femur Datasets

Firstly, first principal stress $_1$ and strain $_1$ distributions in example cases from the femur datasets are shown in Figs. 2 and 3, respectively. Very good correspondence can be seen between the solutions produced using micro-CT- and statistical model-derived material anisotropy.

Figure 2 appears here

Fig. 2 – First principal stress distributions (Pa) computed for two femur datasets using material anisotropy measured from micro-CT (a) and estimated using the proposed statistical approach (b).

Figure 3 appears here

Fig. 3 – First principal strain computed for two femur datasets using material anisotropy measured from micro-CT (a) and estimated using the proposed statistical approach (b).

Subsequently, excellent agreement between the computed fracture loads using the two material models was found in all cases as shown in Fig. 4, with $\rho_c = 98.6\%$. Relative error statistics for the estimates are summarized in Table 2. The average relative error equals 1.7% and all the cases are estimated with less than 4.8% relative errors, which shows the consistency of the technique.

Figure 4 appears here

Fig. 4 – Degree of agreement between the micro-CT (x axis) and the statistical model-based (y axis) fracture load estimates, for the 33 femurs (unit in N).

Examples of the locations of failed elements within the femur models are shown in Fig. 5, where it can be seen that very good agreement concerning the failure regions within the models is produced in each case.

Figure 5 appears here

Fig. 5 – Failed elements for two femur datasets using material anisotropy measured from micro-CT (a) and estimated using the proposed statistical approach (b).

3.2 Vertebra Datasets

Good agreement between the simulation results derived from the micro-CT- and statistical model-based material models was also obtained for the vertebra datasets. Example first principal stress and strain distributions are shown in Figs. 6 and 7, and close correspondence is again observed.

Figure 6 appears here

Fig. 6 – First principal stress distributions (Pa) computed for two vertebra datasets using material anisotropy measured from micro-CT (a) and estimated using the proposed statistical approach (b).

Figure 7 appears here

Fig. 7 – First principal strain computed for two femur datasets using material anisotropy measured from micro-CT (a) and estimated using the proposed statistical approach (b).

In terms of the computation of the fracture loads for the vertabrae, the correlation of fracture load estimates, while slightly lower than for the femur datasets, is very good nonetheless ($\rho_c = 95.5\%$) as shown in Fig. 8. Summary error statistics for the vertebra datasets are presented in Table 3, with an average relative error for the 20 vertebrae of 4.0%. Only a single case was simulated with a relative error over 10%.

Figure 8 appears here

Fig. 8 – Degree of agreement between the micro-CT (x axis) and the statistical model-based (y axis) fracture load estimates, for the 20 vertebrae (unit in N).

Figure 9 show some examples of the locations of failed elements for vertebral datasets, with, again, good agreement concerning the failure regions between the results obtained with micro-CT and by using the proposed statistical estimates of fabric tensor.

Figure 9 appears here

Fig. 9 – Failed elements for two vertebral datasets using material anisotropy measured from micro-CT (a) and estimated using the proposed statistical approach (b).

4   Discussion & Conclusions

In this work, we have demonstrated the viability of estimating patient-specific bone tissue material parameters from clinical images using a statistical model of the tissue microarchitecture. Our approach allows estimation of the distribution of material fabric tensors throughout individual bones, and thereby an estimation of the tissue's mechanical anisotropy. Whereas micro-CT or other similarly high resolution modalities are required to observe and quantify these characteristics directly, our approach requires only relatively low resolution images of the bone, such as from routinely acquired CT. Simulation results using micro-CT- and statistically-based estimates of anisotropy showed excellent agreement. Given the difficulties, both practical and ethical, in

using high resolution modalities in patients, and considering the importance of mechanical ani-sotropy to overall bone function and strength, this capability is significant for patient-specific modeling applications.

As mentioned, the effectiveness of the proposed approach was assessed by means of simula-tions of femur and vertebra models using both micro-CT- and statistical model-derived anisotro-py estimates. In particular, the fracture loads predicted in each case by this means, and for each anisotropy estimate, were compared. Fracture loads were selected as a point of focus given their clear clinical relevance. Though these predictions were based on a well-established methodology [57], it should be noted that even in the case of the micro-CT-based values, they remain in silico estimates only; i.e., no comparisons with real fracture data were made. However, it is important to empahsize that the main goal of the paper is to show that our statistical approach to fabric ten-sor estimation affords biomechanical simulation results of similar accuracy to those obtained when the fabric tensors are measured directly from micro-CT, in other words, verification of the numerical procedure rather than validation of the physical model. Similarly, several failure crite-ria could have been chosen for the computation of the failure loads. However, the comparison remains valid as long as the same criterion was used in both the micro-CT and statistical models. In this work, we performed our calculations using the MPS criterion, which has been shown to be an accurate predictor of failure in experiments with loading configurations that are reasonably similar to those in our simulations [58]. The simulations thus serve the purposes of the present work by demonstrating that in such applications micro-CT-derived material data can, with high confidence, be replaced with data derived from clinically feasible lower resolution images, using our approach.

The use of linear elastic FE analysis to investigate fracture behavior may be similarly consid-ered a limitation of this work. It is commonly considered that bone behaves linear elastic until a 0.7% strain [64, 65]. However, real bone fracture processes may be accompanied by progressive degradation and softening as localized failure of tissue constituents occurs, and real fracture loads are thus likely to differ from those predicted in linear analyses. Continuum damage formal-

ism (e.g. [60]) provides a more robust basis for such investigations. Again, however, our objective in the present work was to verify the effectiveness of the proposed statistical modeling scheme in a simulation context, not to validate any particular model of bone failure. For this purpose, the described linear analyses are suitable.

It is worth noting from the experiments that the performance of the proposed technique for the estimation of the fracture loads is higher for the femur ($\rho_c = 98.6\%$, average relative error of 1.7%) than for the vertebra ($\rho_c = 95.4\%$, average relative error of 4.0%). This is an expected result as the statistical models were trained with more datasets in the case of the femur (32 in the leave-one-out experiments, against 19 for the vertebra), which resulted in a wider coverage of variability and increased prediction accuracy. This is a general limitation of statistical methods, which require by definition representative training samples to increase the quality of the models. While we acknowledge that the number of datasets used in the validation is not very high, it is important that the statistical models perform well even when trained with small training samples due to the difficulties to find large numbers of donors in practice and thus to collect large ex vivo training samples. This is well demonstrated in this paper with the accurate results obtained consistently in all simulations (both femur and vertebra).

Finally, at a time where there is also an increasing interest in the collection and sharing of high resolution ex vivo datasets of bone microarchitectures in the research community (e.g. [44]), we hope this study will also promote the development and use of statistical predictive methods as the one presented in this work for biomechanical simulation of bone structure and function.

Acknowledgment

Conflict of Interest

Bert van Rietbergen is a consultant for Scanco Medical AG.

References

1.   Capture the fracture. Report 2012. International Osteoporosis Foundation, 2012.

2.   Åkesson K., D. Marsh, P. Mitchell, A. McLellan, J. Stenmark, D. Pierroz, C. Kyer, C. Cooper and I. F. W. Group. Capture the fracture: A best practice framework and global campaign to break the fragility fracture cycle. Osteoporosis international 24: 2135-2152, 2013.

3.   Seeman E. and P. D. Delmas. Bone quality—the material and structural basis of bone strength and fragility. New England Journal of Medicine 354: 2250-2261, 2006.

4.   Cummings S. R. and L. J. Melton. Epidemiology and outcomes of osteoporotic fractures. The Lancet 359: 1761-1767, 2002.

5.   Mc Donnell P., P. Mc Hugh and D. O'mahoney. Vertebral osteoporosis and trabecular bone quality. Annals of Biomedical Engineering 35: 170-189, 2007.

6.   Johnell O. and J. Kanis. An estimate of the worldwide prevalence and disability associated with osteoporotic fractures. Osteoporosis international 17: 1726-1733, 2006.

7.   Genant H., P. Delmas, P. Chen, Y. Jiang, E. Eriksen, G. Dalsky, R. Marcus and J. San Martin. Severity of vertebral fracture reflects deterioration of bone microarchitecture. Osteoporosis international 18: 69-76, 2007.

8.   Modlesky C. M., S. Majumdar, A. Narasimhan and G. A. Dudley. Trabecular bone microarchitecture is deteriorated in men with spinal cord injury. Journal of Bone and Mineral Research 19: 48-55, 2004.

9.   Hazrati-Marangalou J., F. Eckstein, V. Kuhn, K. Ito, M. Cataldi, F. Taddei and B. van Rietbergen. Locally measured microstructural parameters are better associated with vertebral strength than whole bone density. Osteoporosis international 25: 1285-1296, 2014.

10.   Travert C., N. Vilayphiou, H. Follet and W. Skalli. Finite element vertebral model for fracture risk prediction: comparison of a full CT-based model versus two media simplified model, a preliminary study. Computer Methods in Biomechanics and Biomedical Engineering 15: 81-82, 2012.

11.   Wang X., A. Sanyal, P. M. Cawthon, L. Palermo, M. Jekir, J. Christensen, K. E. Ensrud, S. R. Cummings, E. Orwoll and D. M. Black. Prediction of new clinical vertebral fractures in elderly men using finite element analysis of CT scans. Journal of Bone and Mineral Research 27: 808-816, 2012.

12.   Derikx L. C., N. Verdonschot and E. Tanck. Towards clinical application of biomechanical tools for the prediction of fracture risk in metastatic bone disease. Journal of biomechanics 48: 761–766, 2015.

13.   Nishiyama K. K., S. Gilchrist, P. Guy, P. Cripton and S. K. Boyd. Proximal femur bone strength estimated by a computationally fast finite element analysis in a sideways fall configuration. Journal of biomechanics 46: 1231-1236, 2013.

14.   Hambli R. and S. Allaoui. A robust 3D finite element simulation of human proximal femur progressive fracture under stance load with experimental validation. Annals of Biomedical Engineering 41: 2515-2527, 2013.

15.   Dragomir-Daescu D., J. Op Den Buijs, S. McEligot, Y. Dai, R. Entwistle, C. Salas, L. J. Melton, III, K. Bennet, S. Khosla and S. Amin. Robust QCT/FEA models of proximal femur stiffness and fracture load during a sideways fall on the hip. Annals of Biomedical Engineering 39: 742-755, 2011.

16.   Tomaszewski P. K., N. Verdonschot, S. K. Bulstra and G. J. Verkerke. A comparative finite-element analysis of bone failure and load transfer of osseointegrated prostheses fixations. Annals of Biomedical Engineering 38: 2418-2427, 2010.

17.   Steiner J. A., S. J. Ferguson and G. H. van Lenthe. Computational analysis of primary implant stability in trabecular bone. Journal of biomechanics 48: 807–815, 2015.

18.   Taylor M. and P. J. Prendergast. Four decades of finite element analysis of orthopaedic devices: Where are we now and what are the opportunities? Journal of biomechanics 2015.

19.   Polikeit A., L. P. Nolte and S. J. Ferguson. The effect of cement augmentation on the load transfer in an osteoporotic functional spinal unit: finite-element analysis. Spine 28: 991-996, 2003.

20.   Cowin S. C. The relationship between the elasticity tensor and the fabric tensor. Mechanics of Materials 4: 137-147, 1985.

21.   Harrigan T. and R. Mann. Characterization of microstructural anisotropy in orthotropic materials using a second rank tensor. Journal of Materials Science 19: 761-767, 1984.

22.   Zysset P. and A. Curnier. An alternative model for anisotropic elasticity based on fabric tensors. Mechanics of Materials 21: 243-250, 1995.

23.   Brandi M. L. Microarchitecture, the key to bone quality. Rheumatology 48: iv3-iv8, 2009.

24.   Dalle Carbonare L. and S. Giannini. Bone microarchitecture as an important determinant of bone strength. Journal of endocrinological investigation 27: 99-105, 2004.

25.   Arlot M. E., B. Burt-Pichat, J. P. Roux, D. Vashishth, M. L. Bouxsein and P. D. Delmas. Microarchitecture influences microdamage accumulation in human vertebral trabecular bone. Journal of Bone and Mineral Research 23: 1613-1618, 2008.

26.   Zysset P., M. Ominsky and S. Goldstein. A novel 3D microstructural model for trabecular bone: I. The relationship between fabric and elasticity. Computer Methods in Biomechanics and Biomedical Engineering 1: 321-331, 1998.

27.   Ding M., A. Odgaard and I. Hvid. Accuracy of cancellous bone volume fraction measured by micro-CT scanning. Journal of biomechanics 32: 323-326, 1999.

28.   Hulme P., S. Boyd and S. Ferguson. Regional variation in vertebral bone morphology and its contribution to vertebral fracture strength. Bone 41: 946-957, 2007.

29.   Sran M. M., S. K. Boyd, D. M. Cooper, K. M. Khan, R. F. Zernicke and T. R. Oxland. Regional trabecular morphology assessed by micro-CT is correlated with failure of aged thoracic vertebrae under a posteroanterior load and may determine the site of fracture. Bone 40: 751-757, 2007.

30.   Boutroy S., M. L. Bouxsein, F. Munoz and P. D. Delmas. In vivo assessment of trabecular bone microarchitecture by high-resolution peripheral quantitative computed tomography. The Journal of Clinical Endocrinology & Metabolism 90: 6508-6515, 2005.

31.   Liu X. S., X. H. Zhang, K. K. Sekhon, M. F. Adams, D. J. McMahon, J. P. Bilezikian, E. Shane and X. E. Guo. High-resolution peripheral quantitative computed tomography can assess microstructural and mechanical properties of human distal tibial bone. Journal of Bone and Mineral Research 25: 746-756, 2010.

32. Burrows M., D. Liu and H. McKay. High-resolution peripheral QCT imaging of bone micro-structure in adolescents. Osteoporosis international 21: 515-520, 2010.

33. Gong H., M. Zhang, Y. Fan, W. Kwok and P. Leung. Relationships between femoral strength evaluated by nonlinear finite element analysis and BMD, material distribution and geometric morphology. Annals of Biomedical Engineering 40: 1575-1585, 2012.

34. Patel T. K., M. D. Brodt and M. J. Silva. Experimental and finite element analysis of strains induced by axial tibial compression in young-adult and old female C57Bl/6 mice. Journal of biomechanics 47: 451-457, 2014.

35. Chappard D., M.-F. Baslé, E. Legrand and M. Audran. Trabecular bone microarchitecture: A review. Morphologie 92: 162-170, 2008.

36. Cowin S. Wolff's law of trabecular architecture at remodeling equilibrium. Journal of Biomechanical Engineering 108: 83-88, 1986.

37. Hazrati-Marangalou J., K. Ito, M. Cataldi, F. Taddei and B. van Rietbergen. A novel approach to estimate trabecular bone anisotropy using a database approach. Journal of biomechanics 46: 2356-2362, 2013.

38. Saha P. K. and F. W. Wehrli. A robust method for measuring trabecular bone orientation anisotropy at in vivo resolution using tensor scale. Pattern Recognition 37: 1935-1944, 2004.

39. Varga P. and P. Zysset. Sampling sphere orientation distribution: an efficient method to quantify trabecular bone fabric on grayscale images. Medical Image Analysis 13: 530-541, 2009.

40. Kersh M. E., P. K. Zysset, D. H. Pahr, U. Wolfram, D. Larsson and M. G. Pandy. Measurement of structural anisotropy in femoral trabecular bone using clinical-resolution CT images. Journal of biomechanics 46: 2659-2666, 2013.

41. Larsson D., B. Luisier, M. E. Kersh, E. Dall'Ara, P. K. Zysset, M. G. Pandy and D. H. Pahr. Assessment of transverse isotropy in clinical-level CT Images of trabecular bone using the gradient structure tensor. Annals of Biomedical Engineering 42: 950-959, 2014.

42. Tabor Z., R. Petryniak, Z. Latała and T. Konopka. The potential of multi-slice computed tomography based quantification of the structural anisotropy of vertebral trabecular bone. Medical engineering & physics 35: 7-15, 2013.

43. Lekadir K., J. Hazrati-Marangalou, C. Hoogendoorn, Z. Taylor, B. van Rietbergen and A. F. Frangi. Statistical estimation of femur micro-architecture using optimal shape and density predictors. Journal of biomechanics 48: 598–603, 2015.

44. Hazrati-Marangalou J., B. v. Rietbergen and K. Ito. Database of femur samples, Eindhoven University of Technology. 2013.

45. Grassi L., N. Hraiech, E. Schileo, M. Ansaloni, M. Rochette and M. Viceconti. Evaluation of the generality and accuracy of a new mesh morphing procedure for the human femur. Medical engineering & physics 33: 112-120, 2011.

46. Bookstein F. L. Principal warps: Thin-plate splines and the decomposition of deformations. IEEE Transactions on Pattern Analysis and Machine Intelligence 11: 567-585, 1989.

47. Freeman W. T., E. C. Pasztor and O. T. Carmichael. Learning low-level vision. International Journal of Computer Vision 40: 25-47, 2000.

48. Zou W. W. and P. C. Yuen. Very low resolution face recognition problem. IEEE Transactions on Image Processing 21: 327-340, 2012.

49. Goodall C. Procrustes methods in the statistical analysis of shape. Journal of the Royal Statistical Society B 53: 285-339, 1991.

50. Pennec X., P. Fillard and N. Ayache. A Riemannian framework for tensor computing. International Journal of Computer Vision 66: 41-66, 2006.

51. Abdi H. Partial least squares regression (PLS-regression). Thousand Oaks, CA: Sage, 2003, p. 792-795.

52. Rosipal R. and L. J. Trejo. Kernel partial least squares regression in reproducing kernel Hilbert space. The Journal of Machine Learning Research 2: 97-123, 2002.

53. Kundu A., S. K. Mitra and P. Vaidyanathan. Application of two-dimensional generalized mean filtering for removal of impulse noises from images. Acoustics, Speech and Signal Processing, IEEE Transactions on 32: 600-609, 1984.

54. Hazrati-Marangalou J., K. Ito, F. Taddei and B. van Rietbergen. Inter-individual variability of bone density and morphology distribution in the proximal femur and T12 vertebra. Bone 60: 213-220, 2014.

55. Polgar K., M. Viceconti and J. Connor. A comparison between automatically generated linear and parabolic tetrahedra when used to mesh a human femur. Proceedings of the Institution of Mechanical Engineers, Part H: Journal of Engineering in Medicine 215: 85-94, 2001.

56. Oñate E., J. Rojek, R. L. Taylor and O. C. Zienkiewicz. Finite calculus formulation for incompressible solids using linear triangles and tetrahedra. International Journal for Numerical Methods in Engineering 59: 1473-1500, 2004.

57. Pistoia W., B. Van Rietbergen, E.-M. Lochmüller, C. Lill, F. Eckstein and P. Rüegsegger. Estimation of distal radius failure load with micro-finite element analysis models based on three-dimensional peripheral quantitative computed tomography images. Bone 30: 842-848, 2002.

58. Schileo E., F. Taddei, L. Cristofolini and M. Viceconti. Subject-specific finite element models implementing a maximum principal strain criterion are able to estimate failure risk and fracture location on human femurs tested in vitro. Journal of biomechanics 41: 356-367, 2008.

59. Hambli R., A. Bettamer and S. Allaoui. Finite element prediction of proximal femur fracture pattern based on orthotropic behaviour law coupled to quasi-brittle damage. Medical engineering & physics 34: 202-210, 2012.

60. Charlebois M., M. Jirásek and P. K. Zysset. A nonlocal constitutive model for trabecular bone softening in compression. Biomechanics and modeling in mechanobiology 9: 597-611, 2010.

61. Gail M. H. Systematic error. In: Encyclopedia of BiostatisticsJohn Wiley & Sons, Ltd, 2005.

62. Kirkup L. and R. B. Frenkel. Systematic errors. In: An Introduction to Uncertainty in MeasurementCambridge University Press, 2006, pp. 83-96.

63. Lawrence I. and K. Lin. A concordance correlation coefficient to evaluate reproducibility. Biometrics 255-268, 1989.

64. Bayraktar H. H., E. F. Morgan, G. L. Niebur, G. E. Morris, E. K. Wong and T. M. Keaveny. Comparison of the elastic and yield properties of human femoral trabecular and cortical bone tissue. Journal of biomechanics 37: 27-35, 2004.

65. Juszczyk M. M., L. Cristofolini and M. Viceconti. The human proximal femur behaves linearly elastic up to failure under physiological loading conditions. Journal of biomechanics 44: 2259-2266, 2011.

List of Tables

1. Table summarizing the properties and parameters of the femur and vertebral datasets used for the simulations.

2. Relative error statistics for the femur datasets between the micro-CT- and statistical model-based fracture load estimates.

3. Relative error statistics for the vertebrae between the micro-CT and estimated fracture loads.

List of Figures

1. Schematic diagram illustrating the main steps involved in the statistical approach for the estimation of fabric tensors, subsequently used in patient-specific biomechanical simulation and fracture load estimation. $\mathbf{X}$ represents the shape and bone density input variables of the statistical model, while $\mathbf{Y}$ represents the output (statistically-predicted) fabric tensors.

2. First principal stress distributions (Pa) computed for two femur datasets using material anisotropy measured from micro-CT (a) and estimated using the proposed statistical approach (b).

3. First principal strain distributions computed for two femur datasets using material anisotropy measured from micro-CT (a) and estimated using the proposed statistical approach (b).

4. Degree of agreement between the micro-CT (x axis) and the statistical model-based (y axis) fracture load estimates, for the 33 femur datasets (units are N).

5. Failed elements for two femur datasets using material anisotropy measured from micro-CT (a) and estimated using the proposed statistical approach (b).

6. First principal stress distributions (Pa) computed for two vertebra datasets using material ani-

    sotropy measured from micro-CT (a) and estimated using the proposed statistical approach

    (b).

7. First principal strain computed for two femur datasets using material anisotropy measured

    from micro-CT (a) and estimated using the proposed statistical approach (b).

8. Degree of agreement between the micro-CT (x axis) and the statistical model-based (y axis)

    fracture load estimates, for the 20 vertebra datasets (units are N).

9. Failed elements for two vertebral datasets using material anisotropy measured from micro-CT

    (a) and estimated using the proposed statistical approach (b).

Table 1. Table summarizing the properties and parameters of the femur and vertebral datasets

used for the simulations.

	Femur	**Vertebra**
Number of datasets	33	20
Female / male	17 / 16	10 / 10
Average age (years)	77.8 ± 10.0	78.0 ± 8.1
Age range (years)	61-95	64-92
Nominal isotropic resolution (μm)	82	37
Filtering	Laplace-Hamming filter: Epsilon = 0.5 voxel Cut-off frequency = 0.4 voxel	Gaussian filter: Sigma = 5 Support = 5 voxels
Thresholding (wrt. the max-	40%	15%

imum value)		

Table 2. Relative error statistics for the femur datasets between the micro-CT- and statistical model-based fracture load estimates.

| Mean	Std	Min	Max	Number of datasets > 10% errors
1.7	1.2	0.3	4.8	0

Table 3. Relative error statistics for the vertebra datasets between the micro-CT- and statistical model-based fracture load estimates.

Mean	Std	Min	Max	Number of datasets > 10% errors
4.0	2.9	0.6	11.9	1
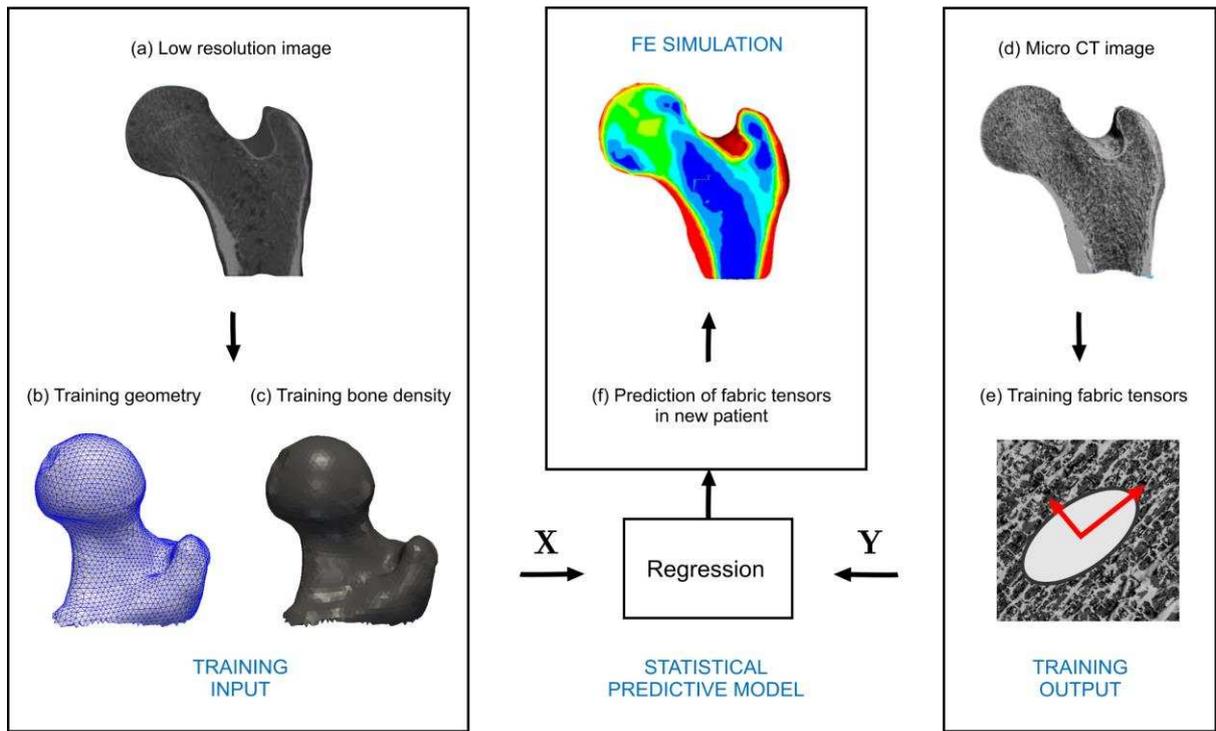
Figure 1
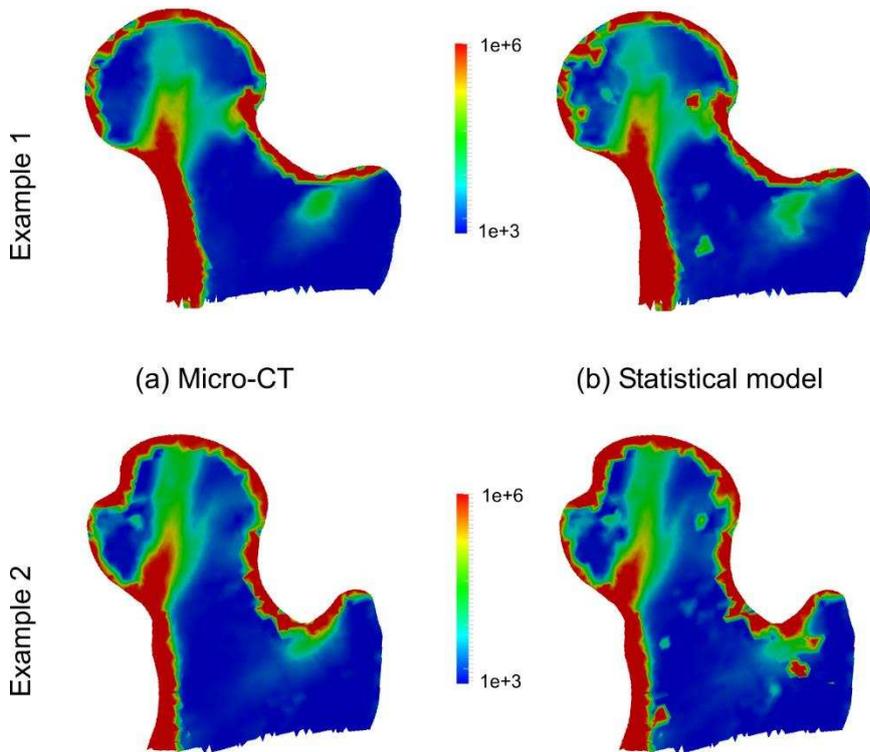
Figure 2

Example 1
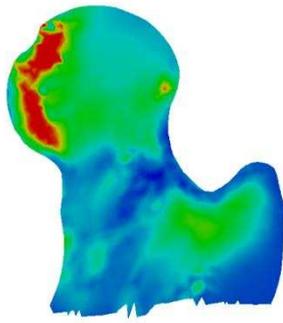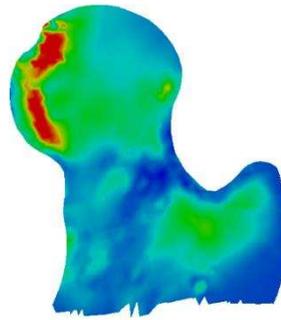
(a) Micro-CT   (b) Statistical model
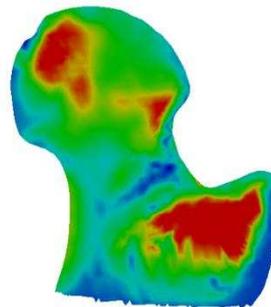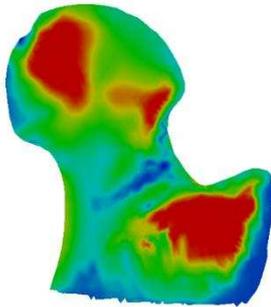
Example 2

Figure 3
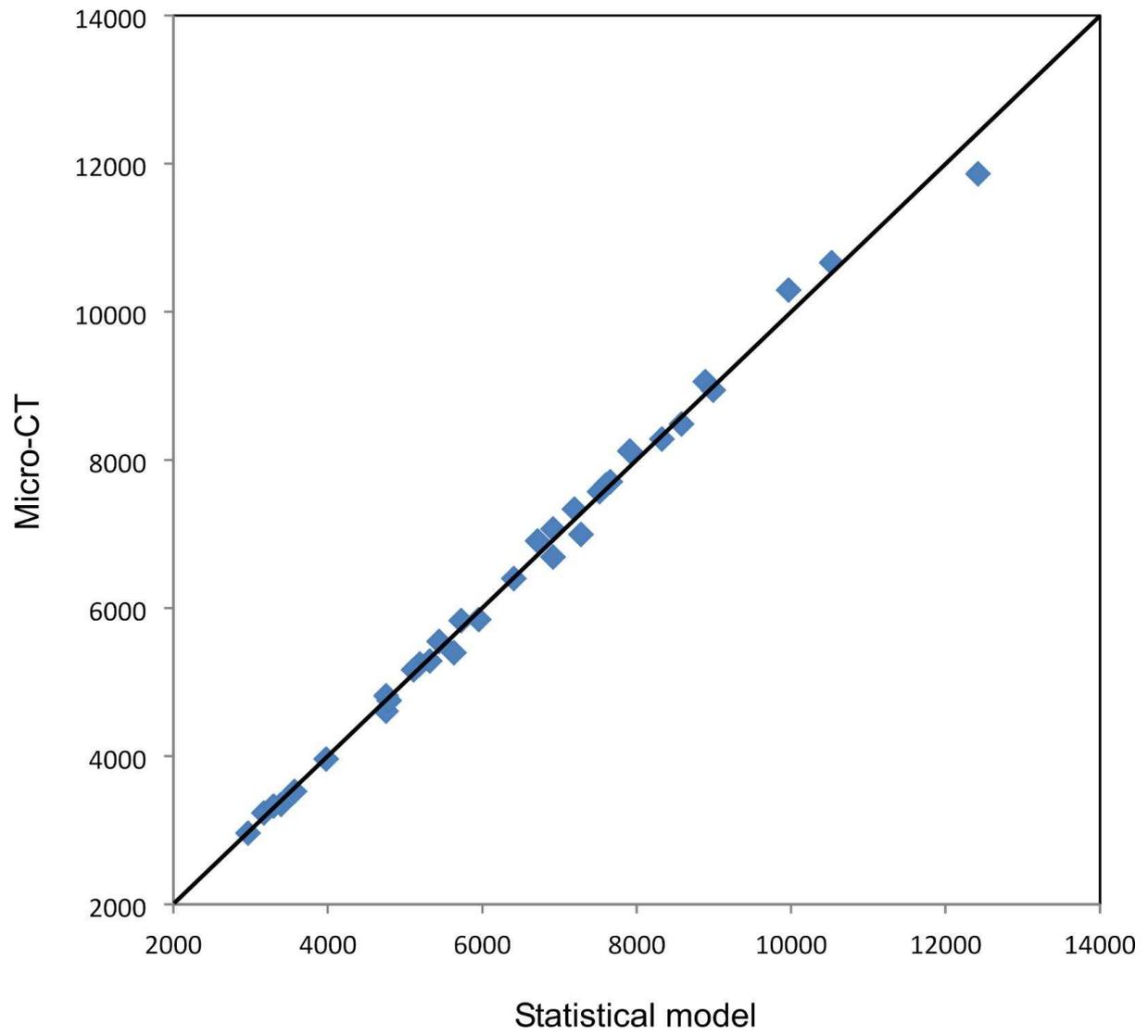
Figure 4

Example 1

(a) Micro-CT

(b) Statistical model

Example 2

Figure 5

Example 1

(a) Micro-CT   (b) Statistical model

Example 2

Figure 6

Example 1

(a) Micro-CT   (b) Statistical model
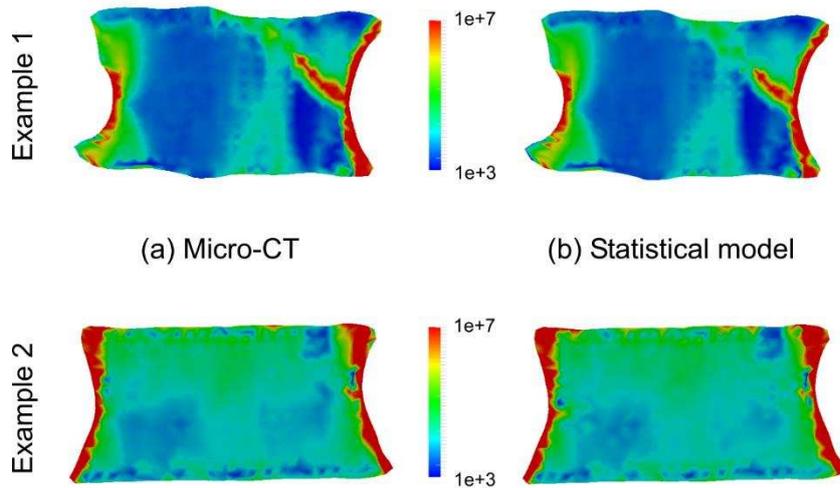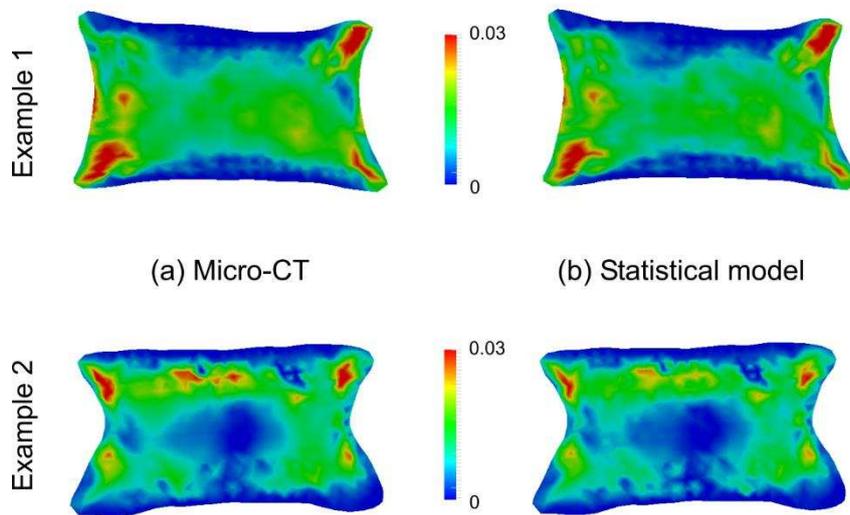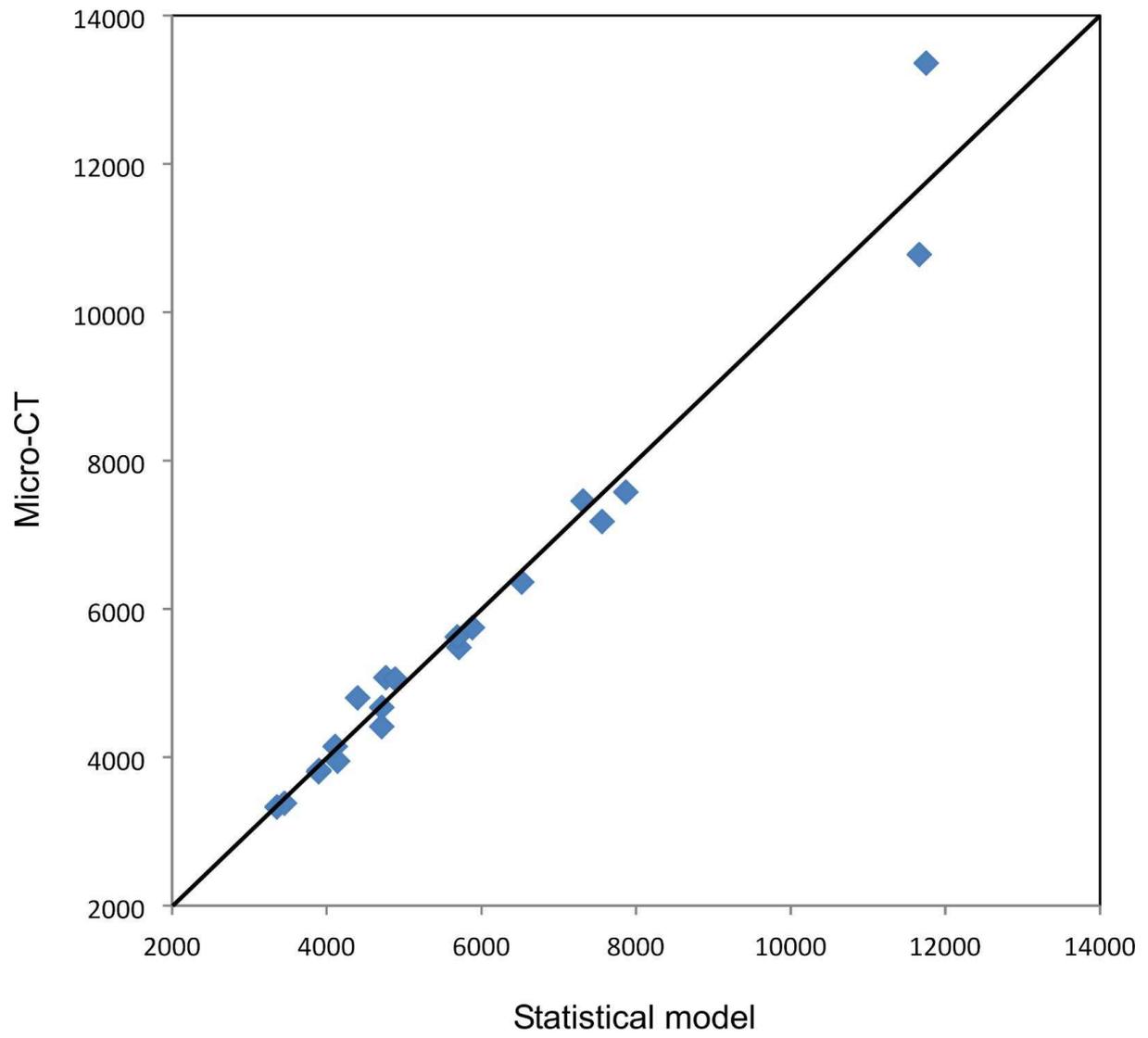
Example 2

Figure 7

Figure 8

Example 1

(a) Micro-CT   (b) Statistical model

Example 2

Figure 9